Journal of Power Sources 225 (2013) 311–315

Contents lists available at SciVerse ScienceDirect

Journal of Power Sources

journal homepage: www.elsevier.com/locate/jpowsour

Short communication

High performance of Ru nanoparticles supported on carbon for anode electrocatalyst of alkaline anion exchange membrane fuel cell

Junya Ohyama [a,b,*], Takuma Sato [a], Atsushi Satsuma [a,b]

[a] Graduate School of Engineering, Nagoya University, Nagoya 464-8603, Japan
[b] Elements Strategy Initiative for Catalysts and Batteries (ESICB), Kyoto University, Katsura, Kyoto 615-8520, Japan

HIGHLIGHTS

- Ru supported on carbon was prepared by reduction of $RuCl_3$ aq. under pH control.
- The smaller Ru nanoparticles exhibited the higher activity to anode electrocatalysts.
- Ru/C with 3 nm metal nanoparticles showed higher cell performance than Pt/C.
- Change of chemical state of Ru/C during fuel cell testing was characterized by XAFS.

GRAPHICAL ABSTRACT

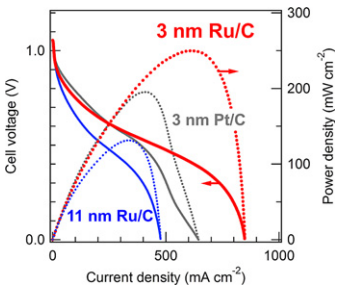

ARTICLE INFO

Article history:
Received 2 July 2012
Received in revised form
1 September 2012
Accepted 13 October 2012
Available online 23 October 2012

Keywords:
Alkaline anion exchange membrane fuel cell
Ruthenium
Anode electrocatalyst
Size-dependent catalytic activity

ABSTRACT

Carbon supported Ru nanoparticles (Ru/C) prepared by liquid phase reduction of $RuCl_3$ by $NaBH_4$ under pH control were applied to anode electrocatalysts of alkaline anion exchange membrane fuel cell (AAEMFC) using hydrogen as fuel. Ru nanoparticles having ca. 3 nm diameter represented higher cell performance than not only Ru/C having large particle size (ca. 11 nm) but also a commercially available Pt/C catalyst. The cell performance of Ru/C increased with the cycle of fuel cell testing. X-ray absorption fine structure spectroscopy analysis indicated that Ru species was reduced during fuel cell testing. Thus, Ru metal can act as highly active site for hydrogen adsorption and oxidation in AAEMFC. The cell testing was also performed using Rh/C, Pd/C, and Ag/C to show that Ru/C was the most active anode catalyst for AAEMFC.

1. Introduction

Proton exchange membrane fuel cells (PEMFCs) are currently the most promising power supplies for various applications from vehicle to mobile phone [1–3]. But, its corrosive environment and demand for high cell performance only allow precious Pt metal to be used as electrocatalysts. Such Pt dependence causes the high cost and prohibits the commercialization of fuel cell system. For reduction of Pt usage, many efforts have been devoted to control the size and surface structure of Pt nanoparticles [4–8]. On the other hand, alkaline anion exchange membrane fuel cells (AAEMFCs) have potential for application of non-Pt metals to electrocatalysts due to the less corrosive environment for the catalysts than PEMFCs [1,9]. Non-Pt metal catalysts such as Pd, Ag, Ni, and manganese oxides have been widely investigated for the cathode electrocatalysts of AAEMFCs [10–13]. However, for the anode electrodes, there are a few studies about non-Pt catalysts [14,15]. This may be due to the high catalytic activity of Pt for hydrogen oxidation reaction. In fact, it has been reported that Pt located at the top of volcano plot of exchange current density of the hydrogen electrode reaction against metal–hydrogen bond energy [16,17]. But the other Pt group metals also showed relatively high exchange current density [16,17].

* Corresponding author. Graduate School of Engineering, Nagoya University, Nagoya 464-8603, Japan. Tel.: +81 52 789 3191; fax: +81 52 789 3193.
E-mail address: ohyama@apchem.nagoya-u.ac.jp (J. Ohyama).

0378-7753/$ – see front matter © 2012 Elsevier B.V. All rights reserved.
http://dx.doi.org/10.1016/j.jpowsour.2012.10.051

Ruthenium is usually used as alloy with Pt anode catalyst to enhance tolerance to CO which emerges as impurity in hydrogen produced by reforming of city gas (CH_4) and as intermediate in direct methanol fuel cell [3,18,19]. Such promotion of catalytic activity and CO tolerance by the alloying is often explained by bifunctional effect. The oxygenated species (OH_{ad}) on Ru reacts with adsorbed CO on Pt through lower energy reaction pathways compared to a Pt catalyst [20–22]. In the bifunctional mechanism, Ru is not considered as an effective site for hydrogen oxidation, which is possibly due to high oxophilicity of Ru. In other words, the preferentially formed Ru–OH_{ad} blocks the adsorption of H_2 [21]. On the other hand, electrochemical oxidation of CO proceeds on a Ru-monometallic catalyst [21,23]. It was reported that a Ru catalyst showed higher electrocatalytic activity for CO oxidation than Pt and Pt–Ru alloy catalysts [21,23]. Thus, if a Ru catalyst shows high catalytic activity to hydrogen oxidation reaction comparable to that of Pt, Ru-based catalysts can become candidates for Pt-free anode catalysts.

In this study, we applied Ru nanoparticles supported on carbon (Ru/C) to anode catalyst of AAEMFC using hydrogen as fuel. In order to achieve high catalytic performance on Ru/C, small Ru nanoparticles were synthesized in a pH-controlled aqueous solution. The structure of Ru/C was characterized by means of X-ray diffraction, transmission electron microscopy (TEM), and X-ray absorption fine structure (XAFS) spectroscopy. To our knowledge, this is the first report to show higher performance of Ru than Pt as an anode catalyst.

2. Experimental

The chemical reagents used in this study were purchased from Kishida Chemical Co., Ltd. unless described otherwise. A series of Ru/C (50 wt% Ru loading) was prepared by liquid phase reduction of $RuCl_3$ using $NaBH_4$ in the presence of carbon black (CB), Vulcan XC-72R: To a 300 mL of $RuCl_3$ aq. (3.3 mmol L^{-1}) containing 10 mL of 2-propanol (for well dispersion of carbon) was added NaOH aq. (0.1 mol L^{-1}) to control the pH from 2 to 10, followed by addition of 100 mg of Vulcan XC-72R; The suspension was reduced with 100 mL of $NaBH_4$ (10 mmol) aq.; After stirring for 0.5 h, the suspension was filtered and the residue was washed with 200 mL of water; The resulting black powder was dried at 353 K overnight. As a reference, Pd/C (50 wt% metal loading) was synthesized by the same method as Ru/C without 2-propanol and pH control using $PdCl_2$ precursor. Rh/C (50 wt%) was also prepared as a reference by reduction of $RhNO_3$ (0.97 mmol) in a mixture of ethylene glycol (100 mL) and water (100 mL) at 393 K for 3 h in the presence of CB (100 mg). The resulting Rh/C suspension was filtered, washed with 200 mL of water, and dried at 353 K. Ag/C (50 wt%) was prepared by physical mixture of Ag nanopowder (Aldrich) and Vulcan XC-72R in a mortar for 5 min. Pt/C (46 wt%) was purchased from Tanaka Kikinzoku Kogyo (TKK).

XRD patterns of Ru/C catalysts were recorded on a Rigaku MiniFlex II/AP diffractometer with Cu $K\alpha$ radiation. Crystallite size of Ru/C was evaluated from the half-width of Ru(0001) line by Scherrer equation after correcting for instrumental peak broadening using the half-width of Si(111) of a silicon powder. The Scherrer constant was assumed to be 0.9. The Ru particle size analysis was carried out by observation using HITACHI H-800 transmission electron microscope operated at 200 kV. The X-ray absorption fine structure (XAFS) measurement at Ru–K edge was carried out on BL01B1 beamline of SPring-8 with a Si(311) two-crystal monochromator. The XAFS samples were in membrane (described below) without Pt/C cathode catalysts, which was cut and stacked to have enough X-ray adsorption for extended XAFS (EXAFS) analysis. Data reduction of XAFS spectra was performed using REX2000 program Ver. 2.5.9 (Rigaku Corp.).

A Ru/C catalyst ink was prepared by ultrasonically dispersion of a suspension containing 25.3 mg of catalysts, 130 mg of 2-propanol, and 220 mg of ionomer solution (AS-4 solution, Tokuyama Corp.). In the same way, Pt/C ink was also prepared using 158 mg of catalysts, 2.37 g of 2-propanol, 0.2 g of water, and 1.36 g of ionomer solution. The prepared inks were applied to anion exchange membranes (A-201, Tokuyama Corp.) to load 0.5 mg_{Ru} cm^{-2} of Ru/C on anode electrode and 0.5 mg_{Pt} cm^{-2} of Pt/C as cathode electrode. The geometric surface area of electrode was 4.84 cm^2.

The prepared membrane electrode assemblies (MEAs) were sandwiched between two carbon papers (AvCarb P50T, Ballard Power Systems), and placed in a single cell (FC05-01SP, Electro Chem. Inc.). Fuel cell testing was carried out at 323 K with H_2 and O_2 (flow rates: 500 ml min^{-1}) supplied at atmospheric pressure to the anode and cathode, respectively. The gas lines between the humidifiers and the fuel cell fixture were heated at 343 K to minimize condensation in the supply pipes. Cell voltage (V_{cell}/V) and power density (P_{cell}/mW cm^{-2}) vs current density (i_{cell}/mA cm^{-2}) curves were collected on a potentiostat (HZ-5000 (HAG-3001), Hokuto Denko Corp.) with another potentiostat (HZ-5000 (HAG-3010), Hokuto Denko Corp.) as a power supply. Before the i–V_{cell} curves were recorded, MEAs were conditioned by operating at 100 mV until the current density had stabilized at a constant value (for ca. 0.5 h).

3. Results and discussion

Fig. 1 shows TEM images of Ru/C (Ru loading: 50 wt%) prepared by $NaBH_4$ reduction of $RuCl_3$ aqueous solution containing 2-prpopanol in the presence of carbon black under pH control (pH = 7) using NaOH aqueous solution and without pH control (pH = 2). We denotes Ru/C prepared under pH = 7 and 2 as Ru/C-A and Ru/C-B, respectively. The particle sizes of Ru nanoparticles of Ru/C-A and Ru/C-B were 3.1 ± 1.3 nm and 10.8 ± 8.5 nm, respectively. XRD patterns (Figure S1) also indicated that Ru/C-A has smaller Ru metal nanoparticles than Ru/C-B. The Ru metal crystallite size of Ru/C-B calculated from the line around 44° derived from Ru(0001) by using Scherrer equation was 10.5 nm, which was well consistent with the size evaluated by TEM, although the size of Ru/C-A was not able to be evaluated from the XRD because of its broad lines and the contribution of that derived from carbon black around 42°. It should be mentioned that the pH control method gave various size of Ru metal nanoparticles, which were indicated by the half-width of the line derived from Ru(0001) (Figure S1), and the smallest Ru metal nanoparticles were obtained under pH = 7. In other words, the size-controlled synthesis of Ru nanoparticles supported on carbon was attained by the pH control of Ru precursor solution.

Fig. 2 shows the cell voltage and power density vs current density curves obtained with MEAs containing Ru/C-A and Ru/C-B (the amount of Ru on each MEA: 0.5 mg_{Ru} cm^{-2}) on anode electrodes and Pt/C (0.5 mg_{Pt} cm^{-2}) as cathode electrodes. As a control, we also performed fuel cell testing using Pt/C (0.5 mg_{Pt} cm^{-2}) as an anode electrode. Ru/C-A exhibited the higher maximum power density than Ru/C-B. This result indicates that smaller Ru nanoparticles have the higher activity to the hydrogen oxidation reaction (HOR). Furthermore, Ru/C-A represented higher performance than Pt/C. It is suggested that Ru can also act as highly active species for the HOR even in the anode condition of AAEMFC, i.e., in the presence of abundant OH^-, although Ru has been considered as less active metal for the HOR than Pt due to the high oxophilicity [21]. One of possible reasons for the higher performance of Ru/C-A than Pt/C is the larger surface area per unit weight of Ru/C-A compared to Pt/C owing to the lower molecular weight of Ru than Pt, which would lead high diffusion limitation current density. But, the low activation overpotential of Ru/C-A comparable to Pt/C

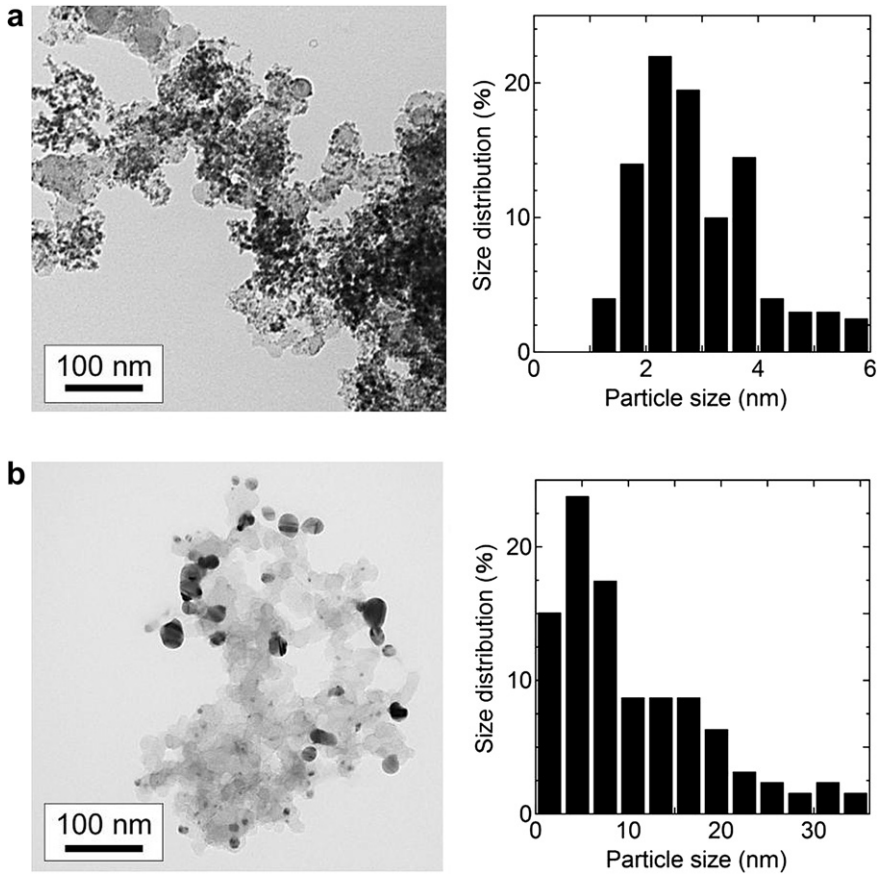

Fig. 1. TEM images of (a) Ru/C-A and (b) Ru/C-B with histograms of particle size.

(see the almost the same I–V curve of Ru/C-A and Pt/C from 0 to ca. 250 mA cm^{-2} of current density) cannot be explained only with the high surface area of Ru/C-A. Such high activity of Ru/C-A for the HOR might be stem from the nanosized structure of Ru, which is now under investigation using a rotating disk electrode method (Figures S2 and S3).

Interestingly, the diffusion limited current density of Ru/C-A largely increased with the cycle of i–V_{cell} measurement from as shown in Fig. 3, although such a phenomenon was not observed when Pt/C was used as an anode electrocatalyst (Figure S3). One of the possible reasons for the enhancement of diffusion limited current is the increase in the number of active sites for the HOR by the variation of chemical state and/or structure of Ru nanoparticles during the cell testing. Thus, we investigated the structure and chemical state of Ru by means of XAFS spectroscopy. Fig. 4 shows the Ru–K edge X-ray absorption near edge structure

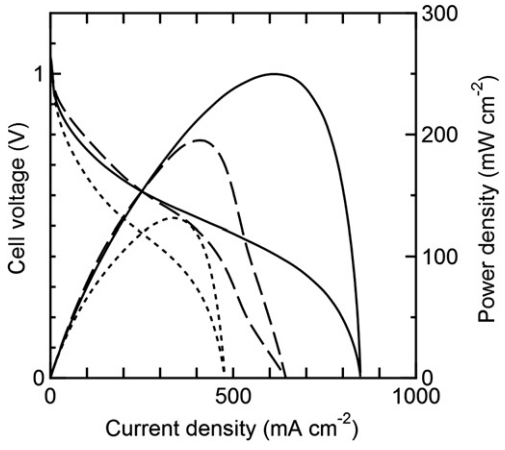

Fig. 2. Cell voltage and power density vs current density curves obtained with MEAs containing Ru/C-A (solid line) and Ru/C-B (dotted line) (the amount of Ru on each MEA: 0.5 mg$_{Ru}$ cm^{-2}) on anode electrodes and Pt/C (0.5 mg$_{Pt}$ cm^{-2}) as cathode electrodes, together with i–V and i–P curves obtained using Pt/C (dashed line) (0.5 mg$_{Pt}$ cm^{-2}) as an anode electrode.

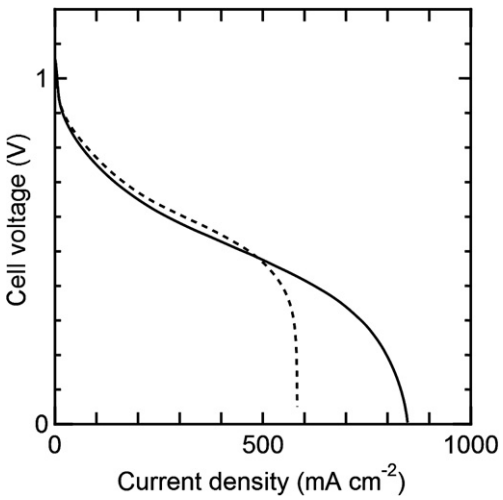

Fig. 3. I–V curves of Ru/C-A obtained at 1st (dotted line) and 50th cycle (solid line) of the measurement.

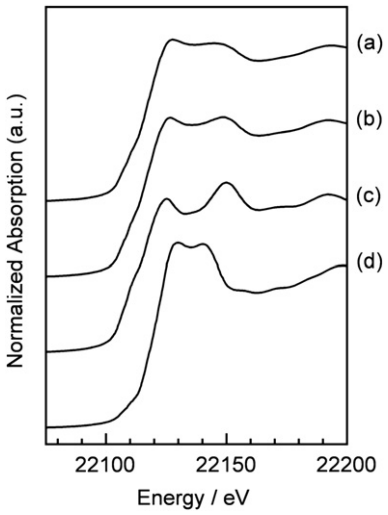

Fig. 4. XANES spectra of Ru/C-A in membrane (a) before the cell testing (Ru/C-A1) and (b) after 50 cycles of the measurement (Ru/C-A2), together with those of (c) Ru foil and (d) RuO_2 as references.

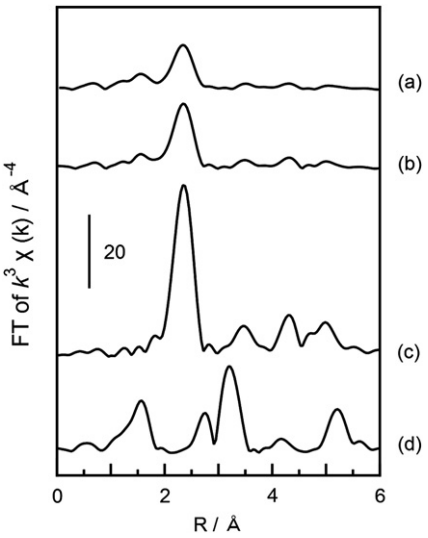

Fig. 5. Fourier transformation of k^3-weighted Ru–K edge EXAFS spectra of (a) Ru/C-A1, (b) Ru/C-A2, (c) Ru foil, and (d) RuO_2.

(XANES) spectra of Ru/C-A in membrane before the cell testing (Ru/C-A1) and after 50 cycles of the measurement (Ru/C-A2) together with those of Ru foil and RuO_2 as references. The XANES spectra of Ru/C-A1 and Ru/C-A2 were fitted by linear combination of the reference spectra to evaluate the Ru metal composition as listed in Table 1. The Ru metal composition of Ru/C-A2 was higher than that of Ru/C-A1, suggesting that Ru species is reduced during the cell testing. On the other hand, the Fourier transformed EXAFS spectra shown in Fig. 5 were analyzed to obtain the structural parameters as listed in Table 1. The backscattering amplitude and phase shift for the Ru–Ru shell at 2.33 Å were obtained by FEFF calculation [24] for a Ru–Ru pair with 2.68 Å of distance. The coordination numbers of Ru–Ru pair (CN (Ru–Ru)) of the samples were corrected by the ratio of known CN (Ru–Ru) of Ru foil (12) to that obtained by the above curve fitting analysis. The corrected CN (Ru–Ru) was reduced by respective Ru metal composition to evaluate the intrinsic CN (Ru–Ru) of Ru metal. As a result, Ru/C-A1 and Ru/C-A2 had almost identical intrinsic CN (Ru–Ru) of Ru metal. Thus, the particle size of Ru did not change in the cell testing. From the CN (Ru–Ru), the size was estimated to be ca. 3 nm in diameter, [25,26] which was well consistent with the size evaluated by the TEM analysis (Fig. 1).

The Ru nanoparticles with 3 nm have ca. 25% of surface Ru atom in a particle, assuming spherical Ru nanoparticles. The XANES analysis described above presented that Ru/C-A1 and Ru/C-A2 has 39 and 27% of RuO_2 (Table 1), which were larger than and almost the same as the surface atom fraction of Ru nanoparticles with 3 nm, respectively. It is suggested that Ru/C-A1 had RuO_2 in bulk, but the oxides was reduced during the fuel cell testing. The surface Ru oxide species of Ru/C-A2 might be formed by air exposure for the ex situ XAFS measurement. Thus, Ru nanoparticles with the oxide can be reduced under the anodic condition of AAEMFCs, and the resulting Ru metal nanoparticles represent the high catalytic activity for the HOR. It is speculated that the formation of Ru–OH_{ad} species does not significantly prevent adsorption of H_2. A detailed study on the HOR on Ru nanoparticles is now under way.

The fuel cell testing was also carried out on MEAs containing various metal (Rh, Pd, Ag) supported on CB catalysts (M/C: M denotes metal) as anode electrode (0.5 mg_{metal} cm^{-2}) and Pt/C (0.5 mg_{Pt} cm^{-2}) as cathode electrode. Table 2 lists the sizes and preparation methods of metal nanoparticles of M/C used in this study. The maximum power densities obtained on the various M/C were plotted against the dissociative chemisorption energy for H_2 on the fcc (211) surface using DFT calculation by Nørskov et al. [27] As shown in Fig. 6, the cell performance tended to increase with the absolute value of the dissociative chemisorption energy for H_2, $|E_{M-H}|$, which is the same result as previously reported relation between exchange current density and E_{M-H} [16,17,28]. Accordingly, only Pt group metals (Ru, Rh, Pd, and Pt) are the candidates for monometal supported on CB catalyst for anode of AAEMFC. In particular, Ru is the most promising metal to substitute for Pt among non-Pt metals.

Table 1
Composition of Ru species analyzed by Ru–K edge XANES spectra[a] and curve fitting results of the EXAFS spectra for Ru–Ru scattering of Ru/C-A1 and Ru/C-A2.[b]

	Composition analysis (%)[a]		Curve fitting analysis[b]				Normalized CN[g]	Intrinsic CN of Ru metal[h]
	Ru	RuO_2	CN[c]	r/Å[d]	σ/Å[e]	R (%)[f]		
Ru/C-A1	61	39	4.9	2.67	0.087	9	6.3	10.4
Ru/C-A2	72	28	6.0	2.67	0.082	5	7.7	10.7
Ru foil	100	0	9.3	2.67	0.66	5	12	12

[a] Evaluated by linear combination fitting of XANES spectra of samples with XANES spectra of Ru foil and RuO_2.
[b] Inverse-Fourier range, r = 2.0–2.7 Å; fitting range, k = 3.8–15.3 $Å^{-1}$.
[c] Coordination number of Ru–Ru.
[d] Interatomic distance.
[e] Debye–Waller factor.
[f] So called R factor.
[g] Normalized with CN of Ru foil = 12.
[h] Calculated by division of normalized CN by Ru composition.

Table 2
List of sizes and preparation method of metal nanoparticles supported on carbon used in this study.

Catalyst	Preparation method	Size/nm
Ru/C-A[a]	$NaBH_4$ reduction at pH = 7	3.1
Ru/C-B[a]	$NaBH_4$ reduction at pH = 2	10.8
Pt/C[a]	Supplied from TKK	2.5
Pd/C[b]	$NaBH_4$ reduction	4.9
Rh/C[b]	Ethylene glycol reduction	3.5
Ag/C[b]	Physical mixing	35

[a] Mean particle size evaluated from TEM.
[b] Crystallite size evaluated from XRD using Scherrer equation.

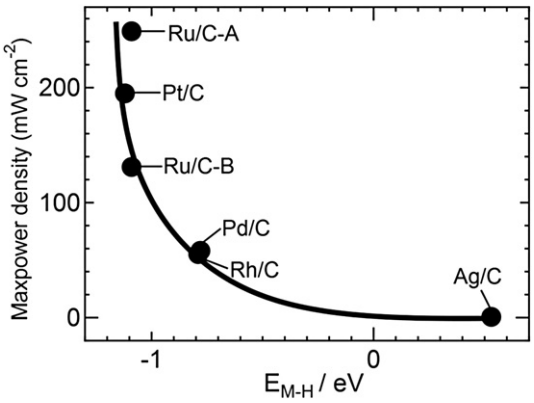

Fig. 6. A plot of maximum power density obtained on MEAs having various metal nanoparticles supported on carbon as anode electrodes (cathode: Pt/C) against the dissociative chemisorption energy for H_2, $|E_{M-H}|$ [27].

4. Conclusion

Carbon supported small Ru nanoparticles with ca. 3 nm diameter was prepared by $NaBH_4$ reduction of $RuCl_3$ aq. containing 2-propanol under pH = 7 to apply the anode electrocatalyst for AAEMFC using hydrogen as fuel. The small Ru nanoparticles represented higher cell performance than large Ru nanoparticles (10.8 ± 8.5 nm). The cell performance of Ru/C increased during the fuel cell testing, when RuO_x species of Ru/C were reduced to Ru metal. It is suggested that the increase in Ru metal contributes to the enhancement of performance during the cell testing. The fuel cell testing was also performed using Pt/C, Rh/C, Pd/C and Ag/C as anode electrocatalysts. The power density obtained on the various metal catalysts tended to increase with $|E_{M-H}|$, and Ru/C having small metal nanoparticles showed higher performance than Pt/C. Therefore, although Ru has been considered as less active metal than Pt, nanosized Ru metal can act as highly active species for the HOR in AAEMFCs.

Acknowledgement

This study was supported by Grant-in-Aid from the Ministry of Education, Culture, Sports, Science and Technology, Japan. The authors thank Dr. Seiji Yamazoe and Dr. Saburo Hosokawa for XAFS measurement, Dr. Shigeo Arai and Dr. Yuta Yamamoto for TEM observation, and Prof. Tsukasa Torimoto (Nagoya Univ.) and Mr. Shin Watanabe (Tokuyama Corp.) for advice about electrocatalysis of Ru and fuel cell testing.

Appendix A. Supplementary data

Supplementary data related to this article can be found at http://dx.doi.org/10.1016/j.jpowsour.2012.10.051.

References

[1] L. Carrette, K.A. Friedrich, U. Stimming, Fuel Cells 1 (2001) 5.
[2] M.A.J. Cropper, S. Geiger, D.M. Jollie, J. Power Sources 131 (2004) 57.
[3] C. Song, Catal. Today 77 (2002) 17.
[4] N.M. Markovic, S.T. Sarraf, H.A. Gasteiger, P.N. Ross, J. Chem. Soc.-Faraday Trans. 92 (1996) 3719.
[5] S. Mukerjee, J. Appl. Electrochem. 20 (1990) 537.
[6] S. Mukerjee, S. Srinivasan, M.P. Soriaga, J. McBreen, J. Electrochem. Soc. 142 (1995) 1409.
[7] C.V. Rao, B. Viswanathan, J. Phys. Chem. C 114 (2010) 8661.
[8] Y. Sun, Y. Dai, Y. Liu, S. Chen, PCCP 14 (2012) 2278.
[9] J.R. Varcoe, R.C.T. Slade, Fuel Cells 5 (2005) 187.
[10] S.N.S. Goubert-Renaudin, A. Wieckowski, J. Electroanal. Chem. 652 (2011) 44.
[11] J. Guo, A. Hsu, D. Chu, R. Chen, J. Phys. Chem. C 114 (2010) 4324.
[12] L. Mao, D. Zhang, T. Sotomura, K. Nakatsu, N. Koshiba, T. Ohsaka, Electrochim. Acta 48 (2003) 1015.
[13] M. Shao, T. Yu, J.H. Odell, M. Jin, Y. Xia, Chem. Commun. 47 (2011) 6566.
[14] K. Asazawa, K. Yamada, H. Tanaka, A. Oka, M. Taniguchi, T. Kobayashi, Angew. Chem. Int. Ed. 46 (2007) 8024.
[15] S.F. Lu, J. Pan, A.B. Huang, L. Zhuang, J.T. Lu, Proc. Natl. Acad. Sci. U S A 105 (2008) 20611.
[16] B.E. Conway, B.V. Tilak, Electrochim. Acta 47 (2002) 3571.
[17] H. Kita, J. Electrochem. Soc. 113 (1966) 1095.
[18] L. Carrette, K.A. Friedrich, U. Stimming, ChemPhysChem 1 (2000) 162.
[19] A. Faur Ghenciu, Curr. Opin. Solid-State Mater. Sci. 6 (2002) 389.
[20] T.-Y. Chen, T.-L. Lin, T.-J.M. Luo, Y. Choi, J.-F. Lee, ChemPhysChem 11 (2010) 2383.
[21] H.A. Gasteiger, N.M. Markovic, P.N. Ross, J. Phys. Chem. 99 (1995) 8290.
[22] C. Lu, R.I. Masel, J. Phys. Chem. B 105 (2001) 9793.
[23] T. Kawaguchi, W. Sugimoto, Y. Murakami, Y. Takasu, Electrochem. Commun. 6 (2004) 480.
[24] A.L. Ankudinov, B. Ravel, J.J. Rehr, S.D. Conradson, Phys. Rev. B 58 (1998) 7565.
[25] R.B. Greegor, F.W. Lytle, J. Catal. 63 (1980) 476.
[26] J. Ohyama, K. Teramura, S.-i. Okuoka, S. Yamazoe, K. Kato, T. Shishido, T. Tanaka, Langmuir 26 (2010) 13907.
[27] T. Bligaard, J.K. Nørskov, S. Dahl, J. Matthiesen, C.H. Christensen, J. Sehested, J. Catal. 224 (2004) 206.
[28] B.E. Conway, G. Jerkiewicz, Electrochim. Acta 45 (2000) 4075.